# Primary hyperparathyroidism caused by parathyroid-targeted overexpression of cyclin D1 in transgenic mice

*See related Commentary on pages 1079–1080.*

Yasuo Imanishi,[1] Yoshitaka Hosokawa,[2] Katsuhiko Yoshimoto,[1] Ernestina Schipani,[2] Sanjay Mallya,[1] Alexandros Papanikolaou,[1] Olga Kifor,[3] Takehiko Tokura,[1] Marilyn Sablosky,[1] Felicia Ledgard,[1] Gloria Gronowicz,[1] Timothy C. Wang,[2] Emmett V. Schmidt,[2] Charles Hall,[1] Edward M. Brown,[3] Roderick Bronson,[4] and Andrew Arnold[1]

[1]University of Connecticut School of Medicine, Farmington, Connecticut, USA
[2]Massachusetts General Hospital, Boston, Massachusetts, USA
[3]Brigham and Women's Hospital, Boston, Massachusetts, USA
[4]US Department of Agriculture Human Nutrition Research Center on Aging at Tufts University, Boston, Massachusetts, USA

Address correspondence to: Andrew Arnold, Center for Molecular Medicine, University of Connecticut School of Medicine, 263 Farmington Avenue, Farmington, Connecticut 06030-3101, USA.
Phone: (860) 679-7640; Fax: (860) 679-7639; E-mail: aarnold@nso2.uchc.edu.

Yasuo Imanishi's present address is: Department of Internal Medicine, Osaka City University Graduate School of Medicine, Osaka, Japan.
Yoshitaka Hosokawa's present address is: Division of Molecular Medicine, Aichi Cancer Center Research Institute, Nagoya, Japan.
Katsuhiko Yoshimoto's present address is: Otsuka Department of Molecular Nutrition, The University of Tokushima School of Medicine, Tokushima, Japan.
Timothy C. Wang's present address is: University of Massachusetts Medical Center, Worcester, Massachusetts, USA.
Yasuo Imanishi, Yoshitaka Hosokawa, and Katsuhiko Yoshimoto contributed equally to this work.

Received for publication June 7, 2000, and accepted in revised form March 19, 2001.

**The relationship between abnormal cell proliferation and aberrant control of hormonal secretion is a fundamental and poorly understood issue in endocrine cell neoplasia. Transgenic mice with parathyroid-targeted overexpression of the *cyclin D1* oncogene, modeling a gene rearrangement found in human tumors, were created to determine whether a primary defect in this cell-cycle regulator can cause an abnormal relationship between serum calcium and parathyroid hormone response, as is typical of human primary hyperparathyroidism. We also sought to develop an animal model of hyperparathyroidism and to examine directly cyclin D1's role in parathyroid tumorigenesis. Parathyroid hormone gene regulatory region–cyclin D1 (*PTH–cyclin D1*) mice not only developed abnormal parathyroid cell proliferation, but also developed chronic biochemical hyperparathyroidism with characteristic abnormalities in bone and, notably, a shift in the relationship between serum calcium and PTH. Thus, this animal model of human primary hyperparathyroidism provides direct experimental evidence that overexpression of the *cyclin D1* oncogene can drive excessive parathyroid cell proliferation and that this proliferative defect need not occur solely as a downstream consequence of a defect in parathyroid hormone secretory control by serum calcium, as had been hypothesized. Instead, primary deregulation of cell-growth pathways can cause both the hypercellularity and abnormal control of hormonal secretion that are almost inevitably linked together in this common disorder.**

*J. Clin. Invest.* **107**:1093–1102 (2001).

## Introduction

A fundamental issue in endocrine cell neoplasia is how two separate properties, abnormal cell proliferation and aberrant control of hormonal secretion, develop and interrelate. Primary hyperparathyroidism, or hypercalcemia due to excessive secretion of parathyroid hormone (PTH) by one or more parathyroid tumors, offers an excellent model system in which this basic problem can be examined. Not only does a proliferative defect leading to parathyroid hypercellularity exist in this common disorder, but studies of pathological parathyroid cells from human parathyroid adenomas in vivo and patients with primary hyperparathyroidism in vivo have revealed abnormalities in the feedback system ("set-point pathway") through which extracellular calcium regulates PTH release (1, 2).

A link between mechanisms controlling proliferation and hormonal production/secretion is also evident in normal parathyroid cells, which respond to the stimulus of chronic hypocalcemia not only by an appropriate homeostatic increase in PTH release but with a secondary expansion of parathyroid cell mass. In fact, it has been hypothesized that most parathyroid tumors are caused by acquired mutation(s) in genes of

the set-point pathway, with this abnormal PTH response to the ambient calcium level actually providing the stimulus to abnormal tumor cell proliferation (3). Whether excess parathyroid endocrine cell proliferation is the result or cause of abnormal hormonal regulation remains controversial.

Two specific genes have been implicated in the pathogenesis of parathyroid adenomas: the *cyclin D1/PRAD1* oncogene (4) and the *MEN1* tumor-suppressor gene (5). Cyclin D1 is an integral component of the cell-cycle regulatory machinery, acting with cyclin-dependent kinases to drive progression through the G1/S checkpoint (6). The *cyclin D1* oncogene is activated in a subset of parathyroid adenomas, in which a chromosome 11 inversion brings the *cyclin D1* gene under the influence of the 5′-regulatory region of the *PTH* gene, leading to cyclin D1 overexpression (4, 7). Cyclin D1 overexpression is found in 20–40% of parathyroid adenomas (8–10). To define the role of cyclin D1 in parathyroid neoplasia and to investigate the relationship between proliferative and hormonal regulatory abnormalities in this disease, we generated transgenic mice that overexpress the *cyclin D1* oncogene in parathyroid glands, using a transgene that mimics the human *PTH–cyclin D1* gene rearrangement.

## Methods

*Transgene construct and generation of transgenic mice.* To target transgene expression to parathyroid tissue, we used the 5′-regulatory region of the human *PTH* gene. This choice was based on the strong and highly restricted tissue specificity of *PTH* gene expression in parathyroid tissue and the clonal juxtaposition of the upstream *PTH* region with *cyclin D1* in human tumors. Because the precise regulatory elements that govern tissue specificity of *PTH* gene expression are unknown, we selected approximately 5 kb of the *PTH* upstream region as the targeting component of the transgene, given that this length would encompass many of the tissue-specific enhancer elements used successfully in transgenic experiments (11–13). Specifically, a 5.2-kb *Bgl*II–*Bgl*II 5′-regulatory fragment of the human *PTH* gene (14) (kindly provided by Henry Kronenberg, Massachusetts General Hospital), consisting of 5.1 kb of flanking sequence and the first 66 bp of untranslated exon 1 (full sequence: GenBank accession number AF346654) was ligated to a 16-kb human genomic *cyclin D1* fragment including all exons and introns, 1.1-kb 5′-flanking region, and 1-kb 3′-flanking region (15). The genomic *cyclin D1* sequence, rather than its cDNA, was chosen to most faithfully represent the *PTH–cyclin D1* gene rearrangement found in human tumors. Because the *cyclin D1* component of the transgene included its own promoter, the transgenic *cyclin D1* transcript was expected to originate from this promoter and to rely on the *PTH* sequences for their longer-range tissue-specific enhancer(s); indeed, sequenced transgene-derived cDNAs from parathyroid tissue contained only cyclin D1 and no contribution from the *PTH* 5′ untranslated region.

This *PTH–cyclin D1* construct was cloned into pBluescript SK$^+$ (Stratagene, La Jolla, California, USA) with synthesized *Nru*I sites in the polylinker region (Figure 1). The 21-kb transgene DNA fragment was released by *Nru*I digestion, isolated by low–melting point agarose gel electrophoresis, and further purified by cesium chloride centrifugation and extensive dialysis. The transgene was microinjected into pronuclei of fertilized eggs from FVB/N mice, and injected eggs were transplanted to pseudopregnant foster mothers and allowed to develop to term. Tail DNA was analyzed by Southern blot analysis using the human *cyclin D1* cDNA as a probe or PCR using the following primers: exon 1A, 5′-GGGGCAGCAGAAGCGAGAGC-3′; exon 1B, 5′-GGGGTGAGTGCAAAGAAAC-3′ (16). All mice were provided with the Prolab RMH 3000 regular diet containing 0.98% calcium and 0.74% phosphorus (PMI Nutrition International, Richmond, Indiana, USA) and water ad libitum. Studies were approved by the appropriate institutional animal care committees at the University of Connecticut Health Center and the Massachusetts General Hospital.

*Histologic examination of parathyroid glands and in situ hybridization.* At necropsy mice were fixed in 10% phosphate-buffered formalin. The thyroid, parathyroids, trachea, esophagus, muscle, and adipose tissue were dissected en bloc, processed, and embedded in paraffin wax. To examine the complete parathyroid glands, serial sections were cut to a thickness of 5 μm and processed either for morphological hematoxylin/eosin or in situ hybridization. In situ hybridization for the human *cyclin D1* gene was performed using complementary antisense and negative control sense $^{35}$S-labeled riboprobes (17), which were transcribed from the plasmid containing the human *cyclin D1* cDNA (pPL-8) (4). Dark-field views were counterstained with hematoxylin and eosin. The histologic identification of parathyroid glands was confirmed by in situ hybridization for *PTH* gene expression using a rat PTH plasmid template and riboprobe.

*Immunohistochemical analysis of cyclin D1 expression.* Immunohistochemical analysis for cyclin D1 was performed on 5-μm-thick frozen tissue sections using the avidin-biotin peroxidase-complex method. Initially, endogenous peroxidase activity in tissue was ablated with 3% hydrogen peroxide in methanol for 5 minutes. Nonspecific protein binding was then suppressed using 10% goat serum for 30 minutes. Tissue sections were incubated overnight at 4°C with biotinylated mouse monoclonal anti-human cyclin D1 Ab at 1:50 dilution (clone 5D4 kindly provided by Masao Seto, Aichi Cancer Center, Nagoya, Japan; commercially available through Immuno-Biological Laboratories, Fujioka, Japan). Characterization and specificity of the Ab has been described elsewhere (18, 19). The next day, slides were washed with PBS. Sections were then incubated with avidin-biotin peroxidase complex at room temperature for 30 minutes using the VectaStain Elite ABC kit (Vector Laboratories, Burlingame, California, USA). 3,3-Diaminobenzidine was used as Chromagen and was applied according to the manufacturer's directions (Roche Molecular Biochemicals, Indianapolis, Indiana, USA). Gill's hematoxylin was used to counter-

stain the tissue. Sections were incubated with PBS in place of primary Ab as negative control.

*RT-PCR analysis of transgene expression*. Total RNA was isolated from multiple tissues in transgenic and wild-type mice. First-strand cDNA was generated using 5 μg total RNA, 200 U of Moloney murine leukemia virus reverse transcriptase (Life Technologies Inc., Rockville, Maryland, USA), and 200 ng of random primers (Life Technologies Inc.) in a total volume of 30 μl. PCR included the following sets of primers. The first set detected expression of the transgene's human *cyclin D1* sequences: sense primer, 5′-GAACAAACAGATCATCCG-CAA-3′ (exon 3), antisense primer, 5′-CCCTTCTGGTAT-CAAAATGC-3′ (exon 5), amplifying a 475-bp fragment during 30 cycles of 60 seconds of denaturation at 94°C, 60 seconds of annealing at 57°C, and 60 seconds of extension at 72°C. RT-PCR for mouse β-actin and mouse PTH were also performed to ensure that the template cDNA was intact and, for the parathyroid/neck region, to confirm the presence of parathyroid-derived RNA/cDNA. Thus, the second primer set detected expression of the mouse PTH gene: sense primer, 5′-GTGATGATCATCATGCTGGCA-3′ (exon 2), antisense primer, 5′-TTTAACTAATACATCCACATC-3′ (exon 3), amplifying a 306-bp fragment during 35 cycles of 60 seconds of denaturation at 94°C, 60 seconds of annealing at 55°C, and extension for 60 seconds at 72°C. The third set detected mouse β-actin gene expression: sense primer, 5′-GTGGGCCGCTCTAGGCACCA-3′, antisense primer, 5′-CGGTTGGCCTTAGGGTTCAGGGGG-3′, amplifying a 244-bp fragment during 30 cycles of 60 seconds of denaturation at 94°C, 45 seconds of annealing at 60°C, and extension for 45 seconds at 72°C. PCR products were analyzed on a 3% agarose gel. The authenticity of RT-PCR products was verified by direct DNA sequencing. These bands were never detected in reactions without reverse transcriptase.

*Assessment of parathyroid cell proliferation using 5′-bromo-2′-deoxyuridine and proliferating cell nuclear antigen*. Two *PTH–cyclin D1* transgenic mice and two wild-type littermates, 10 months old, were fed a standard diet and water containing 5 mg/ml 5′-bromo-2′-deoxyuridine (BrdU; Sigma Chemical Co., St. Louis, Missouri, USA). After 5 days, the mice were sacrificed, and the thyroid-parathyroid complex was dissected, fixed in 4% paraformaldehyde for 1 hour, and saturated overnight with 30% sucrose. The tissue was embedded in OCT medium, and 5-μm-thick axial sections were obtained. Cells that had incorporated BrdU were identified using a BrdU immunostaining kit (Zymed Laboratories Inc., South San Francisco, California, USA). Slides were incubated for 10 minutes in methanol containing 3% hydrogen peroxide to quench endogenous peroxidase and rinsed in PBS for 2 minutes, three times. Sections were digested with 0.1% trypsin for 15 minutes in a moist chamber at 37°C, rinsed in distilled water three times for 2 minutes each time, and incubated for 30 minutes at room temperature with Zymed Laboratories Inc. denaturing solution to denature DNA. The slides were rinsed in PBS for 2 minutes three times and incubated for 15 minutes at room temperature with Zymed Laboratories Inc. blocking solution to reduce nonspecific binding. Sections were then incubated with biotinylated mouse anti-BrdU Ab at room temperature for 2 hours. Excess Ab was rinsed off with PBS, and the bound Ab was detected by the streptavidin-biotin immunoperoxidase method. Sections were stained with diaminobenzidine and counterstained with hematoxylin. Cells with brown nuclear staining were scored as having incorporated BrdU.

Proliferating cell nuclear antigen (PCNA) was detected using a PCNA immunostaining kit (Zymed Laboratories Inc.). Slides were incubated for 10 minutes in methanol containing 3% hydrogen peroxide to quench endogenous peroxidase and rinsed in PBS for 2 minutes, three times. Sections were incubated for 30 minutes at room temperature with Zymed Laboratories Inc. blocking solution to reduce nonspecific binding, followed by incubation with biotinylated mouse anti-PCNA Ab at room temperature for 2 hours. Excess Ab was rinsed off with PBS, and the bound Ab was detected by the streptavidin-biotin-immunoperoxidase method and counterstained as described above. PCNA-positive cells were scored as having brown nuclear staining.

*Bone histology and histomorphometry*. Mice at 22 months of age received intraperitoneal injections of 10 mg/kg of calcein 12 and 2 days before sacrifice. The calvaria were dissected free of tissue, and calvaria were cut in half through the central suture. One-half of the calvaria of each mouse were fixed in 4% paraformaldehyde at 4°C, decalcified in 15% EDTA, dehydrated in increasing concentrations of ethanol, cleared in xylene, and embedded in paraffin. The other half calvaria were fixed in 70% ethanol at 4°C, dehydrated in increasing concentrations of ethanol, cleared in xylene, and embedded in methylmethacrylate. Paraffin-embedded bones were sectioned and 5-μm sections were stained for tartrate-resistant acid phosphatase (TRAP) according to the method of Bancroft (20), and counterstained with hematoxylin. Osteoclasts were identified by TRAP staining and by their characteristic morphology, namely multiple nuclei and localization next to the mineralized matrix. Methylmethacrylate-embedded bones were sectioned, and 5-μm sections were deplastified and left unstained. Sta-

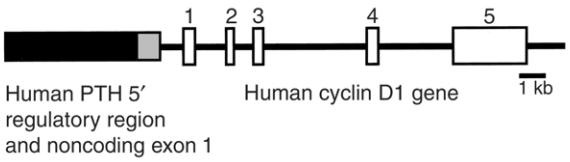


**Figure 1**
Structure of the *PTH–cyclin D1* transgene. The 5.2-kb *Bgl*II–*Bgl*II 5′-regulatory fragment of the human *PTH* gene consists of the 5.1-kb 5′-flanking sequence (black) and the first 66 bp of untranslated exon 1 (gray). The 16-kb human genomic *cyclin D1* component included all five exons, all four introns, 1.1-kb 5′-flanking region, and 1-kb 3′-flanking region.

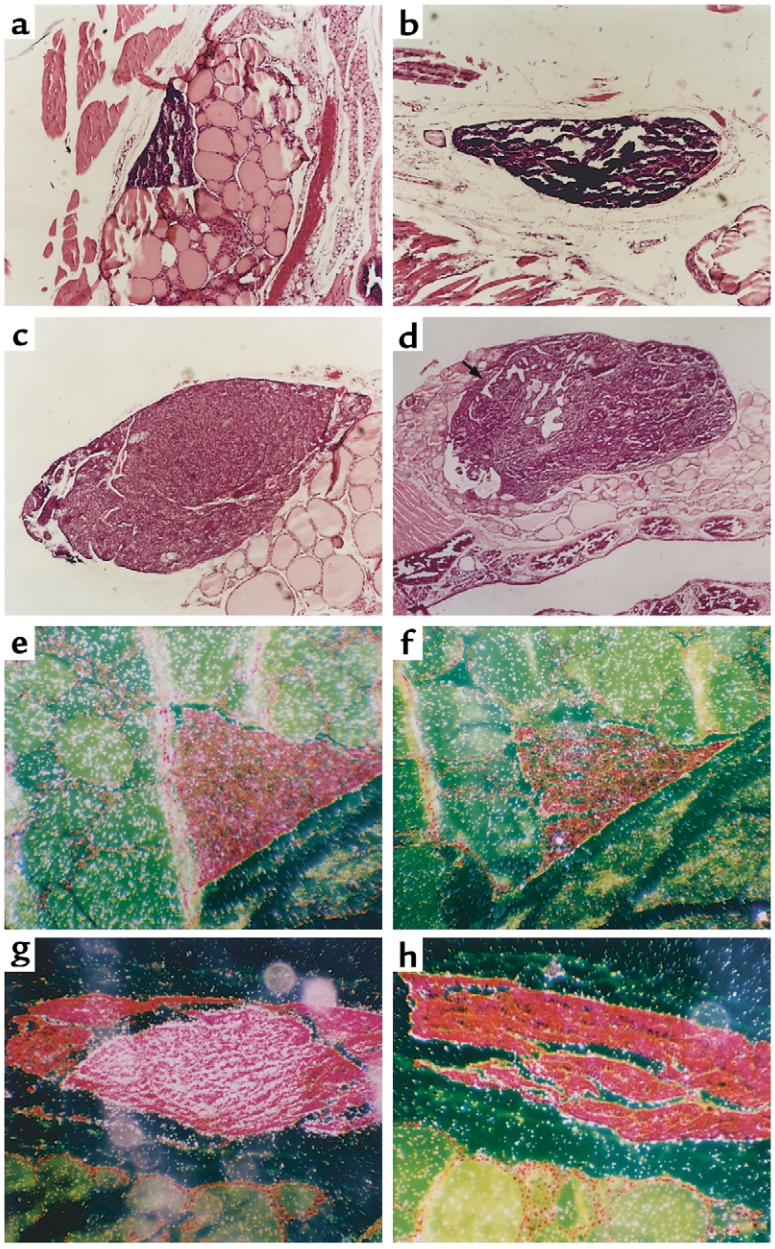


**Figure 2**
Transgene expression and histologic examination of parathyroid glands from *PTH–cyclin D1* transgenic and wild-type mice. Serial sections were cut to a thickness of 5 μm and processed either for morphological hematoxylin/eosin (**a**–**d**) or in situ hybridization (**e**– **h**). (**b**) PC1 mice (×25, 12 months old) and (**c**) PC2 mice (×25, 12 months old) exhibited marked parathyroid hypercellularity in comparison with (**a**) wild-type mice (×25, 12 months old). (**d**) In addition, an example of a gland with the appearance of a parathyroid adenoma with a multilobular pattern is shown (PC2 mouse, 22 months old, ×10). A compressed rim of normal tissue is seen along the left upper face of this tumor (marked with arrow), but not in **a**, **b**, or **c**. In situ hybridization for the human *cyclin D1* gene was performed using complementary $^{35}$S-labeled riboprobes (17), which were transcribed from the plasmid containing the human *cyclin D1* cDNA (pPL-8) (4). Dark-field views counterstained with hematoxylin and eosin are shown. Parathyroid tissue is visualized in pink, and thyroid tissue appears light green. (**e** and **f**) Parathyroid gland from 12-month-old wild-type mouse. (**g** and **h**) Parathyroid gland from 12-month-old PC2 mouse. (**e** and **g**) In situ hybridization with antisense human *cyclin D1* probe. (**f** and **h**) In situ hybridization with negative control sense human *cyclin D1* probe. The histologic identification of parathyroid glands was confirmed by in situ hybridization for *PTH* gene expression using a rat PTH plasmid template and riboprobe (data not shown).

tic and dynamic histomorphometry was performed on 18- to 23-month-old *PTH–cyclin D1* transgenic and wild-type mice. Histomorphometric analyses were performed in a blinded, nonbiased manner using the BIOQUANT computerized image analysis system (BIOQUANT-R & M Biometrics, Nashville, Tennessee, USA). The measurements, terminology, and units that were used for histomorphometric analysis were those recommended by the Nomenclature Committee of the American Society for Bone and Mineral Research (21).

*Blood chemistry analyses*. Blood was collected by tail nicking or by terminal cardiac puncture. Serum calcium levels were measured by a calcium assay (Sigma Chemical Co.) using the *o*-cresolphthalein-complexone method (22). Serum phosphorus, albumin, and creatinine levels were measured by an autoanalyzer. Serum PTH levels were measured using the rat PTH immunoradiometric assay (Nichols Institute, San Juan Capistrano, California, USA).

*Measurement of PTH response to variation in serum calcium concentration*. After fasting 5–6 hours, mice were administered a single intraperitoneal injection of calcium gluconate or EDTA. The doses of calcium gluconate were 75, 150, and 300 μmol/kg body weight (BW). The doses of EDTA were 75, 150, 300, and 500 μmol/kg BW. If hypocalcemia was not achieved with 500 μmol/kg BW, additional doses of EDTA (750 and 900 μmol/kg) were administered. Blood was collected by tail nicking 30 minutes after injection. Serum was collected once a day, on 8 consecutive days for each mouse. Nonlinear mixed effects models were used to fit the sigmoidal curve of Brown (23).

*Immunohistochemical analysis of calcium-receptor expression in parathyroid gland*. Frozen sections of mouse thyroid gland with adherent parathyroid gland(s) were prepared, and those containing parathyroid tissue were identified by standard hematoxylin and eosin staining. The parathyroid gland–containing sections were air-dried at room temperature. After treatment with an endogenous peroxidase inhibitor (DAKO Corp., Carpinteria, California, USA), the slides were blocked with 1% (wt/vol) BSA in PBS for 30 minutes, and immunostaining was performed as

described previously (24, 25) by sequential application of primary antiserum (overnight at 4°C with 5 μg/ml of affinity-purified, polyclonal anti-calcium receptor [anti-CaR] antiserum 4637) and then secondary Ab (1 hour at room temperature with peroxidase-conjugated goat, anti-rabbit IgG) in blocking solution, and finally use of the DAKO 3-amino-9-ethylcarbazole (AEC) substrate system. Photomicrographs were taken at ×100 and ×400. To document the specificity of the immunostaining, the anti-CaR antiserum was preincubated with the peptide against which it was raised (corresponding to amino acids 345–359 of the bovine CaR) before performing immunohistochemistry as just described. Abolition of CaR immunoreactivity when the antiserum had been peptide blocked indicated that the immunostaining was specific for the immunogenic peptide sequence, which is present in all mammalian CaRs examined to date.

## Results

A total of six independent founder *PTH–cyclin D1* transgenic mice were generated, four of which successfully transmitted the transgene to progeny. Three transgenic lines, PC1, PC2, and PC4, were analyzed in this study, selected to represent a range of transgene copy numbers and to assure that any phenotype was qualitatively independent of the specific transgene integration site for that line. The estimated transgene copy numbers of lines PC1, PC2, and PC4 were approximately 3, 11, and 15, respectively (data not shown). Strong expression of the *cyclin D1* transgene in parathyroid tissue was confirmed by using in situ hybridization (Figure 2) and immunohistochemistry (Figure 3). After confirming similarity of the phenotype in all lines (below), PC1 and PC2 lines were selected for further detailed studies.

A survey of other transgenic mouse tissues for expression of the *cyclin D1* transgene was performed by RT-PCR analysis with primers that reside in exons 3 and 5 of the human *cyclin D1* gene (see Methods). Because the primer-binding sequences in the human transgene product are very different from the corresponding region in mouse *cyclin D1*, this assay was designed to specifically detect transcripts from the transgene, as opposed to endogenous murine *cyclin D1* transcripts or product amplified from contaminating genomic DNA; this specificity was confirmed by direct sequencing of the PCR product. The expected expression in the parathyroid/neck region was observed, and no transgene expression was found in any of the other examined tissues including brain, thymus, heart, lung, liver, spleen, kidney and bone/calvaria, with the exception of testis (not shown). The ectopic expression in testis was minimal as it was not detectable by in situ hybridization (not shown); testes from these mice exhibited no histological abnormalities. The thymus was grossly and histologically normal, and no obvious lesions were present in the hypothalamus; these tissues have been reported to express PTH ectopically in native animals (26, 27). Thus, the 5.2-kb 5′-regulatory region of the human *PTH* gene appropriately targets high-level transgene expression specifically to parathyroid cells.

Transgenic and wild-type littermates demonstrated no significant differences in morphology, weight, or growth. The ratio of transgenic to wild-type mice was 1:1, as expected. Transgenic mice grew normally, showed no differences in weight as compared with wild-type mice, have lived longer than 2 years without any sign of abnormality, and were fertile.

Comparisons of biochemical phenotypes across wild-type and transgenic mouse genotypes for 18- to 27-month-old mice (mean ages 21.0–23.1) were done using Kruskal Wallis and Mann-Whitney nonparametric rank tests. PC1, PC2, and PC4 transgenic mice were similar in terms of body weight, serum calcium, phosphorus, creatinine, and PTH levels. Wild-type mice were similar in body weight, serum albumin, and creatinine levels to the transgenic mice, but transgenic mice had significantly higher levels of serum calcium (PC2: median 11.65 mg/dl vs. 9.2 mg/dl, $P < 0.0001$; PC1: median 12.45 mg/dl, $P < 0.001$; PC4: median 11.4 mg/dl, $P < 0.001$) and PTH (PC2: median 140 pg/ml vs. 44 pg/ml, $P = 0.006$; PC1: median 115 pg/ml, $P < 0.001$; PC4: median 150 pg/ml, $P < 0.001$) than wild-type mice. Similarly, PC2 mice also had significantly lower levels of serum phosphorus (median 6.0 mg/dl vs. 7.2 mg/dl, $P = 0.01$) than wild-type mice. In terms of time course, we discerned a trend toward higher calcium and PTH levels in the transgenic mice starting at 4–6 months of age; by 12–13 months of age those differences became

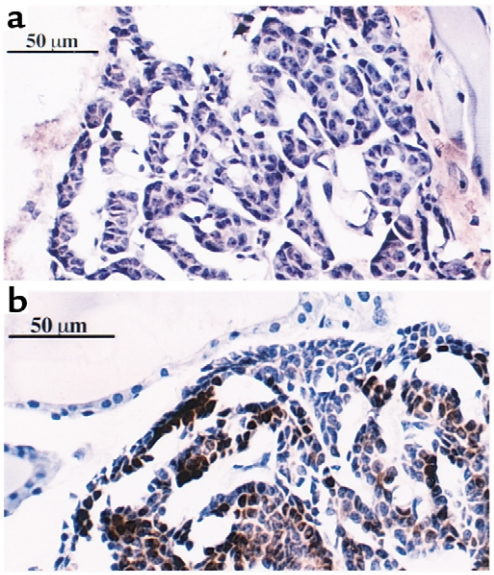


**Figure 3**
Immunohistochemical analysis of cyclin D1 expression. (**a**) Parathyroid gland from a 12-month-old wild-type mouse showing no staining. Parathyroids of wild-type mice were uniformly negative for cyclin D1 staining. (**b**) Parathyroid gland from a 10-month old *PTH–cyclin D1* transgenic (PC2) mouse. Staining (dark brown) is localized to the nucleus and is distributed nonuniformly throughout the parathyroid. Adjacent thyroid tissue is negative for staining. The same pattern of expression was common to other PC2 mice.

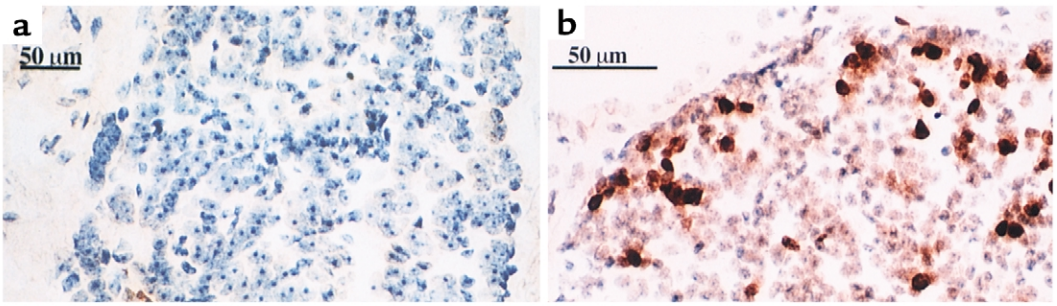


**Figure 4**
Analysis of parathyroid cell proliferation using immunohistochemical detection of BrdU incorporation. (**a**) Wild-type mouse parathyroid, negative for BrdU incorporation. (**b**) *PTH–cyclin D1* transgenic mouse parathyroid with BrdU-positive cells marked by dark-brown nuclear staining. Positive cells were nonuniformly scattered through the gland.

significant (data not shown). All transgenic mice had normal serum creatinine levels indicating that the increased levels of serum calcium and PTH were not due to secondary/tertiary hyperparathyroidism of uremia and that the mild chronic primary hyperparathyroidism did not cause major end-organ damage to the kidneys.

Examination of the parathyroid glands from 1-year-old transgenic mice revealed a marked increase of glandular size and hypercellularity suggesting hyperplasia (Figure 2). Based on the maximum diameter of the glands visualized on serial sections and the number of sections in which the glands were visualized, the size of the parathyroids in transgenic mice was estimated to be increased more than two- to threefold in PC1 and PC2 lines, respectively. Furthermore, in one cohort at ages greater than 18 months, 3 of 11 transgenic PC1 mice and 3 of 11 transgenic PC2 mice exhibited histologic features suggestive of adenoma; Figure 2d shows such an adenomatous-appearing parathyroid with a multilobular, tubular pattern, which was encapsulated, compressed surrounding normal parathyroid tissue, and contained chief cells with more cytoplasm than normal**.** In addition, the size of parathyroid tumors within the same transgenic animal often exhibited considerable asymmetry. In one group of transgenic mice age 19–27 months, 10 of 17 mice (59%) for which two parathyroids could be identified exhibited such asymmetry, raising the possibility of adenomatous outgrowth on the expected hyperplastic cellular milieu. While none of these criteria or observations can be considered proof that a clonal tumor (adenoma) was present, the findings do suggest that it may be fruitful to also seek stochastic acquired alterations in oncogenes/tumor-suppressor genes other than *cyclin D1* as contributors to parathyroid tumorigenesis in these mice, just as is the case for human parathyroid tumors (28). Mitoses, typically found in human parathyroid carcinomas, but not adenomas, were not observed in parathyroid tumors from *PTH–cyclin D1* mice. Neither parathyroid hyperplasia nor apparent adenomas were observed in wild-type mice. Multiple organs of all sacrificed mice were carefully examined, and histological analyses were systematically carried out on 15 transgenic mice, with all other tissues including testis, thymus, brain, kidney, lung, liver, and bone being grossly normal. No osteosarcomas were observed. No metastases were seen.

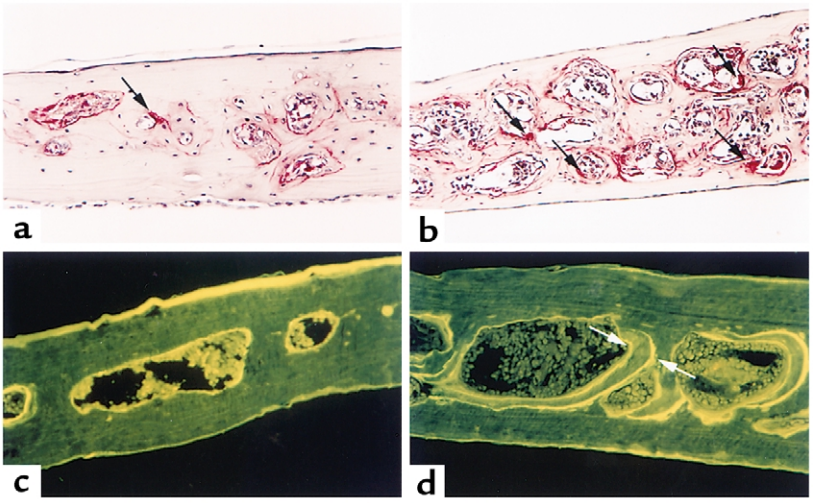


**Figure 5**
Bone histology and histomorphometry in *PTH–cyclin D1* transgenic mice. Paraffin-embedded bones from mice at 22 months of age were sectioned, and 5-μm sections were stained for TRAP according to the method of Bancroft (20) and counterstained with hematoxylin. Osteoclasts were identified by TRAP staining and by their characteristic morphology, namely multiple nuclei and localization next to the mineralized matrix. More osteoclasts (arrows) and marrow spaces were found in the PC2 mice (×225) (**b**) compared with the wild-type mice (×225) (**a**). These images signify increased bone resorption in the PC2 mice. Methylmethacrylate-embedded bones were sectioned, and 5-μm sections were deplastified and left unstained. (**c**) PC2 calvaria (×250) demonstrated wider and increased double-labeled surfaces with wider bands (arrows) in the marrow spaces than the calvaria from wild-type mice (×250) (**d**). The labeling pattern in the PC2 mice suggested increased bone formation.

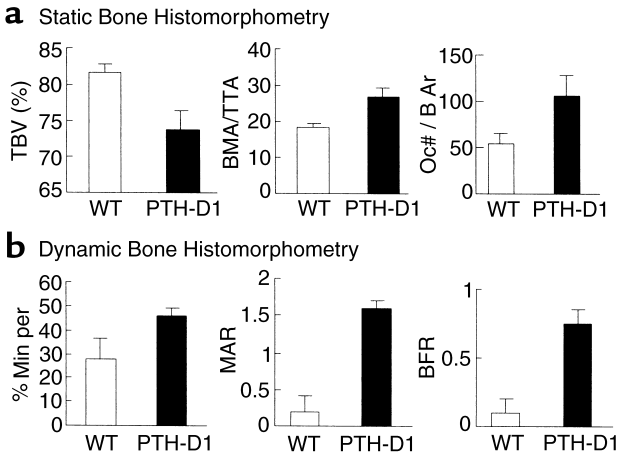


**Figure 6**
Static and dynamic bone histomorphometry in *PTH–cyclin D1* transgenic mice. (**a**) Static and (**b**) dynamic histomorphometry was performed on 18- to 23-month-old *PTH–cyclin D1* transgenic (PTH-D1) and wild-type (WT) mice. For each histomorphometric parameter, PTH-D1 mice were significantly different from WT ($P < 0.05$). Bars, means ± SEM. TBV, total bone volume percentage; BMA/TTA, bone marrow area/total tissue area; OC#/B Ar, osteoclast number/bone area; % Min per, percentage mineralizing perimeter; MAR, mineral apposition rate; and BFR, bone formation rate.

To examine more directly the basis of cyclin D1–induced parathyroid hypercellularity, we assessed parathyroid cell proliferative rates in transgenic mice and controls. First, we compared the incorporation of BrdU in parathyroid cells of *PTH–cyclin D1* mice with that in wild-type littermates. As described in Methods, animals were provided drinking water containing BrdU for 5 days. Proliferating cells that actively incorporated BrdU were identified by immunostaining with an anti-BrdU Ab. Parathyroid tissue from *PTH–cyclin D1* mice showed the presence of numerous BrdU-positive cells scattered throughout the gland in a nonuniform pattern. In contrast, BrdU incorporation was absent in parathyroid glands from wild-type mice (Figure 4). Similar results were obtained with immunostaining with an Ab to PCNA, another marker of cellular proliferation (not shown). Immunostaining patterns for BrdU and PCNA closely matched those for cyclin D1 on contiguous sections (Figures 3 and 4). As an internal control, the majority of the rapidly proliferating basal cells of the esophageal epithelium showed positive dark-brown nuclear BrdU and PCNA immunostaining in both transgenic and wild-type mice (data not shown). Thus, these experiments clearly documented abnormally increased parathyroid-cell proliferation due to parathyroid-targeted overexpression of cyclin D1.

Histomorphometric studies of bone biopsy specimens in patients with primary hyperparathyroidism have demonstrated both a high turnover state and cortical bone loss (29). Compared with wild-type mice, *PTH–cyclin D1* transgenic mice have decreased bone volume and evidence of increased bone turnover with increased numbers of osteoclasts and bone formation in the calvaria (Figure 5). Static histomorphometry showed that 18- to 23-month-old PC2 mice had decreased total bone volume percentage, increased bone marrow area/total tissue area, and increased osteoclast numbers/bone area (Figure 6a). Dynamic histomorphometry for bone formation parameters (Figure 6b) demonstrated that *PTH–cyclin D1* mice had significant increases in percentage of mineralized perimeter, mineral apposition, and bone formation rates compared with the age-matched wild-type mice. This high-turnover phenotype, therefore, had marked similarities with human bone under the influence of excess PTH. No ectopic expression of the cyclin D1 transgene was detected in bone or bone marrow by RT-PCR and immunohistochemical analyses (data not shown), further supporting the conclusion that the bone phenotype was the result of these animals' primary hyperparathyroidism.

We examined the relationship between ambient calcium and parathyroid gland function by determining whether *PTH–cyclin D1* mice could modulate serum PTH levels in response to changes in serum calcium concentration (Figure 7). Negative relationships between serum calcium and PTH were shown for both PC2 and wild-type mice. Linear regression analyses

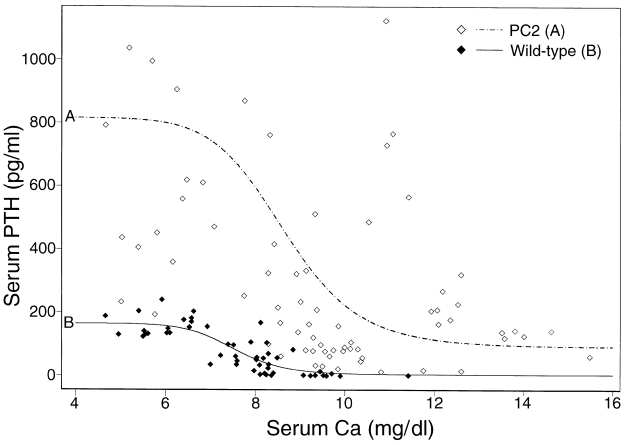


**Figure 7**
Altered PTH response to variation in serum calcium concentration in *PTH–cyclin D1* transgenic mice. After fasting 5–6 hours, mice were administered a single intraperitoneal injection of calcium gluconate or EDTA. The doses of calcium gluconate were 75, 150, and 300 μmol/kg BW. The doses of EDTA were 75, 150, 300, and 500 μmol/kg BW. If hypocalcemia was not achieved with 500 μmol/kg BW, additional doses of EDTA (750 and 900 μmol/kg) were administered. Blood was collected by tail nicking 30 minutes after injection. Serum was collected once a day, on 8 consecutive days, for each mouse. Serum calcium levels were measured by a calcium assay (Sigma Chemical Co.) using the *o*-cresolphthalein-complexone method (22). Observations on PC2 mice are indicated by open diamonds; observations on wild-type mice are indicated by filled diamonds. Nonlinear mixed effects models were used to fit the sigmoidal curve of Brown (23). The dashed line A is the fitted curve for the PC2 mice, excluding one mouse (number 823) with extraordinary values (see Results); the solid line B is the fitted curve for the wild-type mice.

**Figure 8**
CaR immunoreactivity in sections of parathyroid gland from transgenic and wild-type mice. (**a** and **b**) Hematoxylin and eosin staining of a frozen section of a parathyroid gland from a representative transgenic mouse (**a**), again shown to be enlarged, and a wild-type mouse (**b**). The homogeneously staining parathyroid gland in the middle portion of each panel is surrounded by thyroid follicles. ×100. (**c** and **d**) CaR immunoreactivity in the parathyroid glands shown in **a** and **b**, respectively, as assessed using anti-CaR antiserum 4637 and the immunoperoxidase technique as described in Methods. There is rim staining of the parathyroid chief cells from the normal gland (**d**), suggesting expression of CaR protein in the plasma membrane that is substantially more intense than that in the parathyroid gland from the transgenic mouse (**c**). (**e** and **f**) Preabsorption of the anti-CaR antiserum with the peptide against which it was raised abolishes the immunoreactivity (**e**, transgenic; **f**, normal), documenting that the staining is CaR specific. (**c**–**f**) ×400.

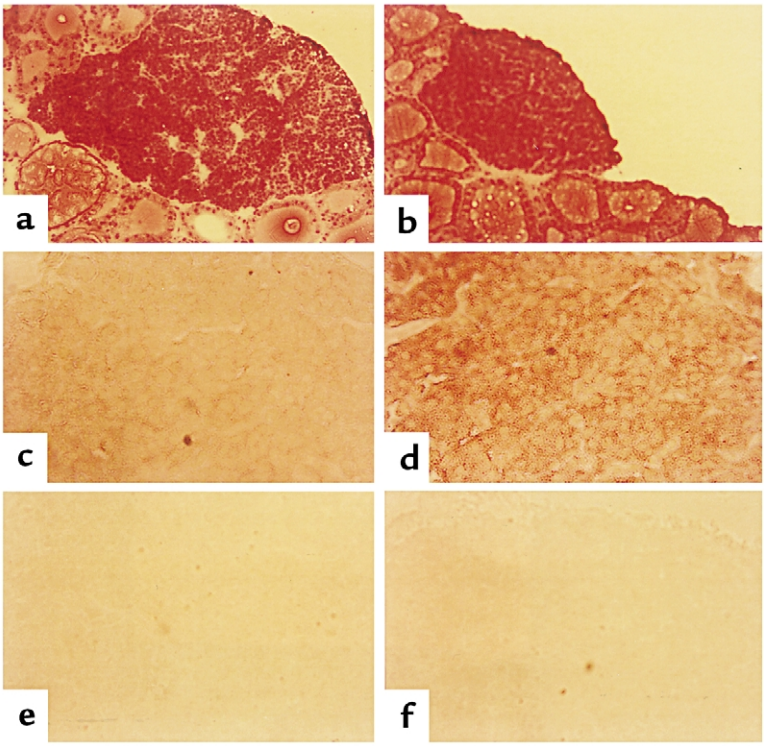


using calcium to predict PTH performed on these data indicated high correlation coefficients: for the six wild-type mice, within-mouse correlations ranged from 0.80 to 0.97, and for the ten PC2 mice the correlations ranged from 0.74 to 0.97. Nine of the ten PC2 mice had an altered relationship, which was shifted upward and to the right and was steeper relative to that in the wild-type mice; the other PC2 mouse, mouse 823, had only three observations recorded, with no serum calcium level below 12.6 mg/dl. There was much greater heterogeneity in the PTH/calcium relationship among the PC2 mice than the wild-type mice, but the direction of the association was the same for all PC2 mice other than the aforementioned mouse 823. The fitted values for the regression lines were larger for every PC2 mouse than for any wild-type mouse for all serum calcium levels less than 9.95 mg/dl; at only one observation at a single time point did any wild-type mouse have a serum calcium level higher than this. The intercepts on the PTH axis were larger ($P = 0.0075$, Mann-Whitney test) and slopes steeper ($P = 0.0075$, Mann-Whitney test) for the PC2 mice (median intercept 837.4 pg/ml at serum calcium 4.0 mg/dl, median slope –116.4) than for the wild-type mice (median intercept 242.4, median slope –43.83). Nonlinear mixed-effects models (30) were used to fit the sigmoidal model of Brown (23) to the PC2 and wild-type mice data; Figure 7 shows the fitted curves. These observations indicate that the abnormal transgenic parathyroids retain the capacity to regulate their secretion of PTH by suppression in the face of enforced increases in serum calcium, and despite the transgenics' baseline hypercalcemia in vivo their parathyroid cells are not at or near a maximally suppressed output of PTH. Thus, the biochemical phenotype of *PTH–cyclin D1* transgenic mice is strongly reminiscent of the abnormalities in calcium-PTH set point determined in vivo in patients with primary hyperparathyroidism (2).

Finally, we examined the level of expression of the CaR in the parathyroids of *PTH–cyclin D1* transgenic mice and controls (Figure 8), because the CaR is a key regulator of calcium-regulated PTH release, and decreased CaR expression has been reported in human parathyroid tumors. The intensity of CaR immunoreactivity was, indeed, substantially less in the transgenic than in the normal parathyroid (Figure 8, c and d, respectively), consistent with reduced expression of receptor protein in the former and comparable to that found in pathological parathyroid glands from patients with primary hyperparathyroidism.

## Discussion

Abnormal cell proliferation and abnormal control of PTH release are concomitant and seemingly omnipresent properties of parathyroid neoplasms. It has been proposed that the only way to explain this concordance, plus the low mitotic rate and long-term clinical/biochemical stability of most parathyroid adenomas is through a primary-acquired mutation in the PTH secretory set-point pathway, with all other described genetic changes being secondary phenomena (3, 31, 32). While it is appealing to speculate that a defect within a set-point control gene could be the major factor leading to parathyroid proliferation in common sporadic primary hyperparathyroidism, no such evidence currently exists. Indeed, the development of parathyroid tumors in transgenic mice with parathy-

roid-targeted *cyclin D1* oncogene overexpression indicates that the hormonal regulatory defect need not be primary, but can result secondary to a primary disturbance in cellular-growth control. Furthermore, the development of this murine model of primary hyperparathyroidism will be a useful tool for genetically dissecting the link between these pathways.

Abnormal regulation of PTH secretion by serum calcium contributes importantly to the pathophysiology of hypercalcemia in parathyroid adenoma (33, 34), and the observed decrease in expression of the CaR in the parathyroid tissue of *PTH–cyclin D1* transgenic mice may well contribute to their increased calcium-PTH set point. Strikingly, this reduction in CaR immunoreactivity appears comparable to that found in pathological parathyroid glands from patients with primary and severe uremic secondary/tertiary hyperparathyroidism (24, 35, 36). Decreased CaR expression is thought to contribute to the elevation in set-point in these two forms of hyperparathyroidism as it does in mice heterozygous or homozygous for targeted disruption of the CaR gene (37) and in humans with inherited inactivating CaR mutations (38). It is of note that severe homozygous or rare heterozygous defects in calcium sensing can also promote parathyroid proliferation (37, 38, 39). However, no primary somatic mutations within the CaR gene have been found in sporadic parathyroid tumors (40), and the mechanism underlying the reduced expression of the CaR in pathological parathyroid glands is not known. Importantly, our observations now provide evidence that cyclin D1 overexpression can induce, directly or indirectly, such a decrease in parathyroid CaR. This finding further validates the *PTH–cyclin D1* mouse as a model of human hyperparathyroidism, and provides an experimental system in which the molecular basis for reduced CaR expression (and/or other components of the set-point pathway) and its role in the pathophysiology of sporadic hyperparathyroidism can be scrutinized.

The development of this transgenic model has additional significance on several fronts. First, the apparent adenomas that evolve in some animals may well be monoclonal neoplasms, and their examination for specific acquired genetic defects — e.g., by loss of heterozygosity (LOH), comparative genomic hybridization, and/or microarray methods — could aid in the identification of cognate genes important in the pathogenesis of human parathyroid adenomas. Second, the successful targeting of transgene expression to the parathyroids indicates that the *PTH* gene's major tissue-specific enhancer(s) lies within the proximal 5 kb of its 5′ regulatory region. Because of the absence of any differentiated parathyroid cell line for use in transfection analyses with reporter constructs, the location of a strong parathyroid-targeting sequence has heretofore remained unknown. The targeting sequence from the *PTH–cyclin D1* transgene should be useful for the selective expression of other gene products in parathyroid tissue, including molecules such as the Cre recombinase to effect tissue-specific knockouts, for example, thereby expanding our opportunities for insights into the physiology and tumor biology of the parathyroids. Third, little is known about the mechanism through which overexpressed cyclin D1 exerts its oncogenicity in the parathyroid tissue context, and *PTH–cyclin D1* mice will permit examination of this issue. Finally, this model provides an attractive system by which the effect of PTH on bone in hyperparathyroid states can be dissected. For example, mice with genetically engineered abnormalities in molecules that are candidates for mediating PTH action on bone could be mated with the *PTH–cyclin D1* transgenic mice and be examined for changes in the bone phenotype. The importance of this issue is heightened by the emergence of osteopenia and diminished bone density as the major indication for treatment of primary hyperparathyroidism in the modern era.


## Acknowledgments

We would like to thank Marcia Nahounou for expert technical assistance, Andrew Karaplis for mouse genomic *PTH*-sequence information, Jonathan Clive for help in data analysis, and Pamela Vachon for invaluable assistance in preparation of the manuscript. This work was supported in part by the NIH grants DK-11794, AR-38933, DK-48330, and DK-52005, the Murray-Heilig Endowment in Molecular Medicine, the Uehara Memorial Foundation (to Y. Hosokawa), The St. Giles Foundation (to E.M. Brown), and an American Cancer Society Faculty Research Award (to A. Arnold).



1. Brown, E.M., Wilson, R.E., Thatcher, J.G., and Marynick, S.P. 1981. Abnormal calcium-regulated PTH release in normal parathyroid tissue from patients with adenoma. *Am. J. Med.* **71**:565–570.
2. Khosla, S., et al. 1993. Calcium infusion suggests a "set-point" abnormality of parathyroid gland function in familial benign hypercalcemia and more complex disturbances in primary hyperparathyroidism. *J. Clin. Endocrinol. Metab.* **76**:715–720.
3. Parfitt, A.M. 1994. Parathyroid growth: normal and abnormal. In *The parathyroids*. J.P. Bilezikian, M.A. Levine, and R. Marcus, editors. Raven Press. New York, New York, USA. 373–405.
4. Motokura, T., et al. 1991. A novel cyclin encoded by a bcl1-linked candidate oncogene. *Nature.* **350**:512–515.
5. Heppner, C., et al. 1997. Somatic mutation of the MEN1 gene in parathyroid tumours. *Nat. Genet.* **16**:375–378.
6. Sherr, C.J. 1996. Cancer cell cycles. *Science.* **274**:1672–1677.
7. Arnold, A. 1995. The cyclin D1/PRAD1 oncogene in human neoplasia. *J. Investig. Med.* **43**:543–549.
8. Hsi, E.D., Zukerberg, L.R., Yang, W.I., and Arnold, A. 1996. Cyclin D1/PRAD1 expression in parathyroid adenomas: an immunohistochemical study. *J. Clin. Endocrinol. Metab.* **81**:1736–1739.
9. Vasef, M.A., Brynes, R.K., Sturm, M., Bromley, C., and Robinson, R.A. 1999. Expression of cyclin D1 in parathyroid carcinomas, adenomas, and hyperplasias: a paraffin immunohistochemical study. *Mod. Pathol.* **12**:412–416.
10. Tominaga, Y., et al. 1999. Expression of PRAD1/cyclin D1, retinoblastoma gene products, and Ki67 in parathyroid hyperplasia caused by chronic renal failure versus primary adenoma. *Kidney Int.* **55**:1375–1383.
11. Hanahan, D. 1985. Heritable formation of pancreatic beta-cell tumours in transgenic mice expressing recombinant insulin/simian virus 40 oncogenes. *Nature.* **315**:115–122.
12. Mellon, P.L., Windle, J.J., and Weiner, R.I. 1991. Immortalization of neuroendocrine cells by targeted oncogenesis. *Recent Prog. Horm. Res.* **47**:69–93.
13. Baetscher, M., Schmidt, E., Shimizu, A., Leder, P., and Fishman, M.C. 1991. SV40 T antigen transforms calcitonin cells of the thyroid but not CGRP-containing neurons in transgenic mice. *Oncogene.* **6**:1133–1138.
14. Vasicek, T.J., et al. 1983. Nucleotide sequence of the human parathyroid hormone gene. *Proc. Natl. Acad. Sci. USA.* **80**:2127–2131.

15. Motokura, T., and Arnold, A. 1993. PRAD1/cyclin D1 proto-oncogene: genomic organization, 5′ DNA sequence, and sequence of a tumor-specific rearrangement breakpoint. *Genes Chromosomes Cancer*. **7**:89–95.
16. Hosokawa, Y., Tu, T., Tahara, H., Smith, A.P., and Arnold, A. 1995. Absence of cyclin D1/PRAD1 point mutations in human breast cancers and parathyroid adenomas and identification of a new cyclin D1 gene polymorphism. *Cancer Lett*. **93**:165–170.
17. Lee, K., et al. 1996. Parathyroid hormone-related peptide delays terminal differentiation of chondrocytes during endochondral bone development. *Endocrinology*. **137**:5109–5118.
18. Banno, S., et al. 1994. Monoclonal antibody against PRAD1/cyclin D1 stains nuclei of tumor cells with translocation or amplification at BCL-1 locus. *Jpn. J. Cancer Res.* **85**:918–926.
19. Nakamura, S., et al. 1994. Immunohistochemical analysis of cyclin D1 protein in hematopoietic neoplasms with special reference to mantle cell lymphoma. *Jpn. J. Cancer Res.* **85**:1270–1279.
20. Bancroft, J. 1990. Enzyme histochemistry. In *The theory and practice of histological technique*. J.D. Bancroft and A. Stevens, editors. Churchill Livingstone. London, United Kingdom. 387–389.
21. Parfitt, A.M., et al. 1987. Bone histomorphometry: standardization of nomenclature, symbols, and units. Report of the ASBMR Histomorphometry Nomenclature Committee. *J. Bone Miner. Res*. **2**:595–610.
22. Sarkar, B.C., and Chauhan, U.P. 1967. A new method for determining micro quantities of calcium in biological materials. *Anal. Biochem*. **20**:155–166.
23. Brown, E.M. 1983. Four-parameter model of the sigmoidal relationship between parathyroid hormone release and extracellular calcium concentration in normal and abnormal parathyroid tissue. *J. Clin. Endocrinol. Metab*. **56**:572–581.
24. Kifor, O., et al. 1996. Reduced immunostaining for the extracellular Ca2+-sensing receptor in primary and uremic secondary hyperparathyroidism. *J. Clin. Endocrinol. Metab*. **81**:1598–1606.
25. Kifor, O., Diaz, R., Butters, R., Kifor, I., and Brown, E.M. 1998. The calcium-sensing receptor is localized in caveolin-rich plasma membrane domains of bovine parathyroid cells. *J. Biol. Chem.* **273**:21708–21713.
26. Nutley, M.T., Parimi, S.A., and Harvey, S. 1995. Sequence analysis of hypothalamic parathyroid hormone messenger ribonucleic acid. *Endocrinology*. **136**:5600–5607.
27. Günther, T., et al. 2000. Genetic ablation of parathyroid glands reveals another source of parathyroid hormone. *Nature*. **406**:199–203.
28. Palanisamy, N., et al. 1998. Novel chromosomal abnormalities identified by comparative genomic hybridization in parathyroid adenomas. *J. Clin. Endocrinol. Metab*. **83**:1766–1770.
29. Parisien, M., et al. 1990. The histomorphometry of bone in primary hyperparathyroidism: preservation of cancellous bone structure. *J. Clin. Endocrinol. Metab*. **70**:930–938.
30. Lindstrom, M.L., and Bates, D.M. 1990. Nonlinear mixed effects models for repeated measures data. *Biometrics*. **46**:673–687.
31. Parfitt, A.M., and Fyhrie, D.P. 1997. Gompertzian growth curves in parathyroid tumours: further evidence for the set-point hypothesis. *Cell Prolif*. **30**:341–349.
32. Parfitt, A.M., Wang, Q., and Palnitkar, S. 1998. Rates of cell proliferation in adenomatous, suppressed, and normal parathyroid tissue: implications for pathogenesis. *J. Clin. Endocrinol. Metab*. **83**:863–869.
33. Birnbaumer, M.E., Schneider, A.B., Palmer, D., Hanley, D.A., and Sherwood, L.M. 1977. Secretion of parathyroid hormone by abnormal human parathyroid glands in vitro. *J. Clin. Endocrinol. Metab*. **45**:105–113.
34. Brown, E.M., et al. 1979. Direct comparison in vivo and in vitro of suppressibility of parathyroid function by calcium in primary hyperparathyroidism. *J. Clin. Endocrinol. Metab*. **48**:604–610.
35. Gogusev, J., et al. 1997. Depressed expression of calcium receptor in parathyroid gland tissue of patients with hyperparathyroidism. *Kidney Int*. **51**:328–336.
36. Farnebo, F., Hoog, A., Sandelin, K., Larsson, C., and Farnebo, L.O. 1998. Decreased expression of calcium-sensing receptor messenger ribonucleic acids in parathyroid adenomas. *Surgery.* **124**:1094–1098.
37. Ho, C., et al. 1995. A mouse model of human familial hypocalciuric hypercalcemia and neonatal severe hyperparathyroidism. *Nat. Genet*. **11**:389–394.
38. Pollak, M.R., et al. 1993. Mutations in the human Ca(2+)-sensing receptor gene cause familial hypocalciuric hypercalcemia and neonatal severe hyperparathyroidism. *Cell*. **75**:1297–1303.
39. Carling, T., et al. 2000. Familial hypercalcemia and hypercalciuria caused by a novel mutation in the cytoplasmic tail of the calcium receptor. *J. Clin. Endocrinol. Metab*. **85**:2042–2047.
40. Hosokawa, Y., Pollak, M.R., Brown, E.M., and Arnold, A. 1995. Mutational analysis of the extracellular Ca(2+)-sensing receptor gene in human parathyroid tumors. *J. Clin. Endocrinol. Metab*. **80**:3107–3110.